applied optics

Flexible geometrical calibration for fringe-reflection optical three-dimensional shape measurement

Ting Yuan,[1,2,*] Feng Zhang,[1] Xiaoping Tao,[1] Xuejun Zhang,[1] and Run Zhou[1,2]

[1]Key Laboratory of Optical System Advanced Manufacturing Technology, Changchun Institute of Optics, Fine Mechanics and Physics, Chinese Academy of Sciences, Changchun, Jilin 130033, China
[2]University of Chinese Academy of Sciences, Beijing 100049, China
*Corresponding author: tingyuano@126.com

Received 17 August 2015; revised 28 September 2015; accepted 28 September 2015; posted 29 September 2015 (Doc. ID 248105); published 23 October 2015

Accurate geometrical calibration is the basis of a fringe-reflection testing system, especially the calibration of reflection ray directions. However, such a calibration procedure is challenging because of two reasons: first of all, the common method of reflection ray directions calibration, which is based on the pinhole camera imaging model, fails in the presence of the pupil imaging aberration. What's more, although using a camera lens with an external stop in front can remove the pupil imaging aberration, it is difficult to achieve the exact geometrical measurement of the camera pinhole and the calibration of the reflection ray directions into the camera because of the low signal-to-noise ratio of images. In this paper, we introduce a new calibration method by finding the points on the liquid crystal display in front of the camera with different positions corresponding to the same camera pixels through correspondence matching. The calibration process and the results from the experiments on fringe-reflection testing demonstrate that the calibration method presented in this paper is simple, practical, and flexible.

OCIS codes: (150.1488) Calibration; (120.6650) Surface measurements, figure; (120.4800) Optical standards and testing; (120.5700) Reflection; (120.2650) Fringe analysis.

http://dx.doi.org/10.1364/AO.54.009102

1. INTRODUCTION

Recently, optical three-dimensional shape measurement based on the fringe-reflection and phase-measuring deflectometry method has been developed rapidly because it has the advantages of being contact-free, and it has a high dynamic range, high accuracy, and can achieve full-field metrology with an easy system setup. In fringe-reflection three-dimensional shape measurement, a liquid crystal display (LCD) screen displays the phase-shift fringe pattern and a camera captures the deformed fringe pattern after specular reflection by the tested specular surface. Häusler *et al.* introduce a microscopic adaptation of deflectometry for measuring the microtopography of specular surfaces [1]. Su *et al.* introduced the software-configurable optical test system (SCOTS), which is a slope measurement technique based on deflectometry, for the testing of the large optical mirrors. SCOTS has good performance in testing many large astronomy telescope mirrors, such as solar reflectors and precision x ray mirrors [2–5].

The major challenge in fringe-reflection three-dimensional shape measurement is the geometrical calibration of optical devices like an LCD screen, camera, and especially, a mirror. Commonly, the reflection ray directions into the camera are calibrated based on the pinhole camera imaging model. But pinhole camera imaging model fails in the presence of the pupil imaging aberration. It means that the entrance pupil would have different locations and shapes for light from different field angles. Su *et al.* removed this effect by using a camera lens with an external stop in the front [3]: the external stop represented the location of the pinhole camera. But it is difficult to accurately calibrate the geometrical parameters, such as focal length, distortion, and so on of the pinhole camera. In addition, the low signal- to-noise ratio of images (especially when the lens has a long focal length) would greatly decrease the accuracy of phase unwrapping or corner data extraction in the camera calibration. So there is a great need to find a method to cope with these problems. In this paper, we introduce a calibration method by using an LCD screen with a dual-frequency crossed fringe in front of the camera. We just need to move the LCD screen once and find the points on the LCD, with different positions corresponding to the same camera pixels by using

correspondence matching. With his method, we can finish the calibration easily during the reflection ray directions calibration of the camera without using an external stop in the fringe-reflection testing system.

2. BASIC PRINCIPLE

A. Principle and Analysis of Fringe-Reflection Test

The schematic diagram of the fringe-reflection testing system is shown in Fig. 1. Figure 1 shows how the surface slope is measured and calculated. An LCD screen displaying fringe patterns that are designed by a computer is set up near the center of curvature (CoC) of the test mirror. The LCD faces toward the mirror. The camera beside the LCD screen will capture the deformed fringe pattern reflected by the mirror. Using the digital phase-shifting technique, the phase information of the deformed fringe pattern can be obtained. Every camera pixel corresponding to a point on the LCD screen can be determined. The principle of fringe reflection can be described simply, as follows: a reflection ray can be determined by camera calibration, such as Zhang calibration [6] and Tsai calibration [7], and an incidence ray can be calibrated by a point on the LCD and the test mirror. With two rays and the coordinates of the LCD screen pixel corresponding to the camera pixel, the mirror pixel, and the camera's center-like point A, B, C in Fig. 1, the surface slopes w_x and w_y in Eq. (1) or α in Fig. 1 can be calculated based on triangulation, which is shown in Eq. (1) [2]. The three-dimension surface shape w can be computed by zonal integration or model iteration [8]:

$$w_x(x_m, y_m) = \frac{\frac{x_m - x_{screen}}{d_{m2screen}} + \frac{x_m - x_{camera}}{d_{m2camera}}}{\frac{z_{m2screen} - w(x_m, y_m)}{d_{m2screen}} + \frac{z_{m2camera} - w(x_m, y_m)}{d_{m2camera}}}$$

$$w_y(x_m, y_m) = \frac{\frac{y_m - y_{screen}}{d_{m2screen}} + \frac{y_m - y_{camera}}{d_{m2camera}}}{\frac{z_{m2screen} - w(x_m, y_m)}{d_{m2screen}} + \frac{z_{m2camera} - w(x_m, y_m)}{d_{m2camera}}}, \quad (1)$$

where x_m and y_m are the coordinates of the test mirror surface, x_{camera} and y_{camera} are the coordinates of the camera, and x_{screen} and y_{screen} are the coordinates of the screen pixel. $z_{m2screen}$ is the z coordinate differences between the mirror and the screen, and $z_{m2camera}$ is the z coordinate differences between the mirror and the camera. $d_{m2screen}$ is the distance between the mirror and the screen, and $d_{m2camera}$ is the distance between the mirror and the camera.

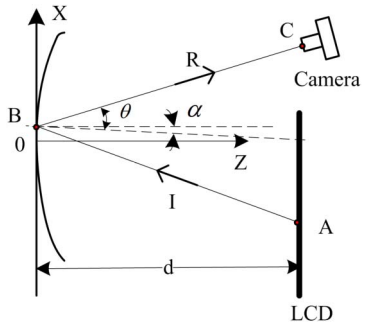

Fig. 1. Principle of slope calculation in fringe-reflection measurement.

Thus, the geometrical calibration in fringe-reflection three-dimensional measurement is aimed to achieve the coordinates of the mirror pixel, LCD screen pixel corresponding to the camera pixel, and the coordinates of the camera center. In Eq. (1), the slopes w_x and w_y are functions of the test mirror surface shape w itself, so we should be able to provide a good initial estimate of the surface shape for the convergence of the implicit function. The sag integrated from the slope can be put back into Eq. (1) to iteratively calculate the slopes and sags with the same method as that commonly used to solve differential equations. We can use the ideal surface shape as the initial estimate of the surface shape. In other words, we can use the cross points of the reflection ray going into the camera and the ideal test mirror surface model as the initial coordinates of the test mirror surface. Before we start, it is necessary that we get the directions of the reflection rays. In [4] and [9], the calibration was performed by assuming a perspective center in the camera model; this work did not consider the pupil imaging aberration issue [4,9]. So the differences between the deviated coordinates of the mirror obtained by these less-precise ray directions and the real coordinates of the mirror cannot be omitted, especially when the distance between the test mirror and camera is relatively long. As a result, the calculated slopes and sags may deviate from the real slopes and sags. Then, in [4], Su *et al.* removed the pupil imaging aberration by using a camera lens with an external stop in the front. They took the center of the external stop as the location of the pinhole camera, and finished the geometry measurement with a laser tracker [4]. There is no doubt that the location and shape of the entrance pupil are well defined in the pinhole camera by using Su Peng's method. But the exact geometrical measurement of the pinhole camera is difficult because the pinhole is too big for the point source microscope [10]. In addition, it is difficult to finish the pinhole camera calibration when the camera lens has a long focal length. The low signal-to-noise ratio and low-contrast images that the pinhole camera captured would decrease the accuracy in either the corner detection or the phase unwrapping.

B. Principle of Geometrical Calibration

In this study, we present a novel calibration method to calibrate the reflection ray directions by using an LCD screen with fringe patterns that are designed by a computer. The screen is placed somewhere in front of the camera and then moved to another location, which is shown in Fig. 2. Screen LCD1, which is in front of the camera, displays the fringe pattern, and the camera captures the fringe pattern at first. Then, we move screen LCD1 along the axis of the test mirror from location 1 to location 2. It is not necessary to know the relationship of the geometrical location between them. The camera records the fringe patterns from the screen, which is located in two different positions. Using the digital phase-shifting technique, the phase information in the fringe pattern can be obtained. Every camera pixel corresponding to a point on screen LCD1 (two different positions, like points A and B) can be determined. So the reflection rays can be determined by the

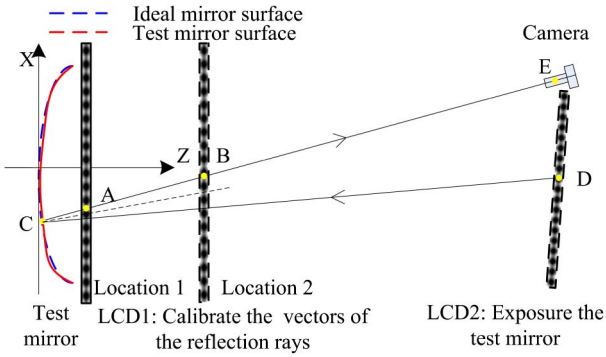

Fig. 2. Schematic of geometrical calibration principle for the fringe-reflection measurement.

points, which correspond to the same camera pixels on the LCD1 located in location 1 and location 2. The accuracy of this method depends on the accuracy of the camera calibration and the LCD screen pixel coordination calibration. In this paper, we use the constraint bundle adjustment [11] to deal with lens distortion and image noise and improve the calibration accuracy of the reflection ray directions. We use a point source microscope [10] to calibrate the coordinates of the LCD screen pixel.

The coordinates of LCD2, which correspond to the camera pixels, can be calibrated by correspondence matching. But the calculated surface normal can vary depending on the assumed surface position even if the incident ray direction and points on LCD2 corresponding to the camera pixels are defined. This issue can be solved by using multiple screen locations (moving the screen to provide ray directions), and prevising the surface shape of the test mirror optics (such as many known points on the test mirror surface), as shown in Fig. 2. Because the mirror shape is roughly on the micron level during the polishing stage of the mirror, we calibrate the coordinates of the mirror by using the precognition surface method, where we use the ideal surface shape as the initial estimate of the actual surface shape.

Because of the existence of the pupil imaging aberration issue, the lens entrance pupil has different shapes and locations, which would interfere with the pinhole camera model. So we cannot use a single point to represent the coordinates of the camera. Here, we replace the coordinates of the camera center with the coordinates of the point on the LCD1 in location 2, and take the ligature line between the points corresponding the same camera pixels on LCD1 in location 1 and location 2 as the reflection ray.

After the geometrical calibration discussed above, the coordinates of the mirror pixel, LCD screen pixel, and camera corresponding to the camera pixel can be obtained. When we put the coordinates into Eq. (1), we can obtain the slope of the test mirror. The integrated sag from the slope calculations can be put back into Eq. (1) to iteratively calculate the slopes and sags.

3. PROCESS OF FRINGE-REFLECTION TEST

A. Correspondence Matching

The purpose of corresponding point matching is to define the points on the LCD screen corresponding to the camera pixels. The absolute phase information of the deformed fringes can be obtained using the digital phase-shift technique and a phase-unwrapping algorithm. The fringe patterns designed by the computer and displayed on the LCD screen are usually a sequence of two orthogonal sinusoidal fringe patterns. But in the fringe-reflection test using the orthogonal sinusoidal fringe, there exists the problem of the sequential process (different fringe directions and phase shifting), and the orthogonal sinusoidal fringe pattern need to be displayed and captured separately. These problems can be completely avoided by using a dual-frequency cross-fringe pattern. Furthermore, a fringe-reflection test or phase measuring deflectometry (PMD) just needs N exposures instead of $2N$ exposures. Therefore, we adopted dual-frequency cross-fringe pattern during the experimental work. The image intensity of the dual-frequency cross-fringe pattern can be described by [12]:

$$I(x,y) = a + b_1\cos[\phi_x(x,y)+\delta_x] + b_2\cos[\phi_y(x,y)+\delta_y]$$
$$\phi_x(x,y) = \frac{2\pi}{T_x}\cdot x,\ \phi_y(x,y) = \frac{2\pi}{T_y}\cdot y,\ \delta_x = n\frac{2\pi}{N},\ \delta_y = nk\frac{2\pi}{N}$$
$$n = 1,\cdots N, N = 5,6,7,\cdots, k = [2, N-2], k \neq N/2, \tag{2}$$

where (x, y) are the pixel coordinates of the LCD screen. For convenience of display, $a = 0.4$, and $b_1 = b_2 = 0.3$. Φ_x and Φ_y are the phase distributions. δ_x and δ_y are the phase shifts. T_x and T_y are the periods of the fringe; they can be the same or different, depending on our need. N is the total number of phase shifts, $2\pi/N$ is the phase step for the x direction, and the fringes are shifted by one period. $2k\pi/N$ is the phase step for the y direction, and the fringes are shifted by k periods.

The practical intensity of the deformed fringes captured by the camera can be denoted by $I_i(u, v)$. $I = 1, 2, \ldots, N$, denotes the phase-shift step, and (u, v) are the coordinates of the camera pixel. The two orthogonal phases can be extracted by:

$$\phi_x(u,v) = -\tan\frac{\sum_{i=1}^{N} I_i \sin\left(i\frac{2\pi}{N}\right)}{\sum_{i=1}^{N} I_i \cos\left(i\frac{2\pi}{N}\right)}$$
$$\phi_y(u,v) = -\tan\frac{\sum_{i=1}^{N} I_i \sin\left(ik\frac{2\pi}{N}\right)}{\sum_{i=1}^{N} I_i \cos\left(ik\frac{2\pi}{N}\right)}. \tag{3}$$

To complete corresponding point matching, a phase-unwrapping algorithm is necessary to recover the absolute phase. Then we can accomplish the correspondence matching according to the property that the absolute phase of a camera pixel is equal to the absolute phase of its corresponding point located on the LCD screen.

B. Image Model and Bundle Adjustment

The purpose of bundle adjustment [11] is to deal with lens distortion and image noise and improve the calibration accuracy of the reflection ray directions. Before bundle adjustment, an imaging model should be considered to describe the practical imaging process. Here, we choose the imaging model of central perspective projection. It can be described by:

$$\lambda\begin{bmatrix} x \\ y \\ 1 \end{bmatrix} = \begin{bmatrix} F_x & 0 & C_x \\ 0 & F_y & C_y \\ 0 & 0 & 1 \end{bmatrix}[R \quad T]\begin{bmatrix} X \\ Y \\ 1 \end{bmatrix}, \tag{4}$$

where λ is the scale factor, $[x, y]$ are the coordinates of the image, and $[X, Y, Z]$ are the coordinates of a point on the LCD1 in the world coordinate frame. For the point located on a plane, $Z = 0$. F_x and F_y are the horizontal and vertical focal length in a pixel unit, and (C_x, C_y) are the coordinates of the principal point. To better describe the practical imaging model, we add the radial and tangential distortions into the model to describe the aberration, and the practical image coordinate is the sum of ideal imaging point (x, y) and aberration $(\delta x, \delta y)$. The aberration can be described by:

$$\delta x = k_1 r_d^2 + k_2 r_d^4 + k_5 r_d^6 + 2k_3 x_d y_d + k_4(r_d^2 + 2x_d^2),$$
$$\delta y = k_1 r_d^2 + k_2 r_d^4 + k_5 r_d^6 + k_3(r_d^2 + 2y_d^2) + 2k_4 x_d y_d, \quad (5)$$

where $x_d = (x - C_x)/F_x$, $y_d = (y - C_y)/F_y$, $r_d^2 = x_d^2 + y_d^2$, and k_1, k_2, k_3, k_4, k_5 denote the distortion coefficients.

The objective of bundle adjustment is $\min[\sum_i(\Delta_{ix}^2 + \Delta_{iy}^2)]$, where Δ_{ix}, Δ_{iy} are the re-projection error of one point. This can be written as

$$\Delta_{ix} = \Re(F_x, F_y, C_x, C_y, k_1, k_2, k_3, k_4, k_5, X_i^w) - x_{\text{real}},$$
$$\Delta_{iy} = \Re(F_x, F_y, C_x, C_y, k_1, k_2, k_3, k_4, k_5, X_i^w) - y_{\text{real}}. \quad (6)$$

where x_{real} and y_{real} are the real coordinates extracted from the image. The bundle adjustment model can be described by:

$$\begin{cases} \min\left[\sum_i(\Delta_{ix}^2 + \Delta_{iy}^2)\right] \\ \rho_i(X_i^w) = X_i^w - [\gamma r_{i1} + (r_{i2} - r_{i1})], \end{cases} \quad (7)$$

$$\begin{bmatrix} \alpha^T\alpha & \beta^T \\ \beta & 0 \end{bmatrix}\begin{bmatrix} \Delta\varpi \\ \Delta\kappa \end{bmatrix} = -\begin{bmatrix} g_i(\varpi_n) \\ \rho_i(\kappa_n) \end{bmatrix}$$
$$\alpha = [\alpha_1, \alpha_2, \cdots \alpha_i]^T,\ \beta = \left[\frac{\partial\rho_1}{\partial X_1^w}, \frac{\partial\rho_1}{\partial X_2^w}, \cdots \frac{\partial\rho_1}{\partial X_i^w}\right]^T$$
$$\alpha_i = \left[\frac{\partial g_i}{\partial F_x}, \frac{\partial g_i}{\partial F_y}, \frac{\partial g_i}{\partial C_x}, \frac{\partial g_i}{\partial C_y}, \frac{\partial g_i}{\partial k_1}, \frac{\partial g_i}{\partial k_2}, \frac{\partial g_i}{\partial k_3}, \frac{\partial g_i}{\partial k_4}, \frac{\partial g_i}{\partial k_5}, \frac{\partial g_i}{\partial X_1^w}, \frac{\partial g_i}{\partial X_2^w}, \cdots \frac{\partial g_i}{\partial X_i^w}\right], \quad (8)$$

where γ is a scale factor that need not be computed. $\varpi = [F_x, F_y, C_x, C_y, k_1, k_2, k_3, k_4, k_5, X_1^w, X_2^w, \cdots X_i^w]^T$ is the parameter to be adjusted in constraint bundle adjustment. $\Delta\varpi$, $\Delta\kappa$ are the adjusted parameters. ϖ, κ can be computed by iteration:

$$\varpi_{n+1} = \varpi_n + \Delta\varpi$$
$$\kappa_{n+1} = \kappa_n + \Delta\kappa. \quad (9)$$

The initial value of κ is set as zero, and the initial value of ϖ is the linear solution of the camera parameters and three-dimensional coordinates.

4. EXPERIMENT AND RESULTS

Now, we perform our experiment. The preliminary experimental setup is shown in Fig. 3. We applied the proposed calibration method in testing a small spherical mirror with a crossed fringe where both of the fringe periods in the two orthogonal directions are 50, and $N = 8$ and $k = 2$. Figure 4 shows a dual-frequency crossed fringe displayed on the LCD screen. As shown in Fig. 3, the dual-frequency crossed fringe generated by the computer is displayed on the DELLP2415Q LCD screen, whose resolution is 3480 pixels × 2160 pixels. The pixel pitch is 0.13725 mm. A virtual image of the fringe in the test mirror is captured by a camera, whose resolution is 1024 pixels × 1280 pixels. The pixel size is 14 μm × 14 μm. In order to calibrate the directions of the reflection rays into camera and get the coordinates of the test mirror, we utilize an LCD displaying a dual-frequency crossed fringe and move screen LCD1 along the test mirror axis once. Then, the virtual images of the fringe are captured by the camera. Some reference points and re-projection points on the CCD image are shown in Fig. 5. After extracting the reference points with sub-pixel precision by the phase-shift method and calibrating the camera by the constraint bundle adjustment method, we use the method to complete the calibration with a group of reflection rays, and then achieve another group of reflection rays by linking the points corresponding the same camera pixels on LCD1 at location 1 and location 2. The impact of the calibration aberration and pupil imaging aberration can be revealed by the

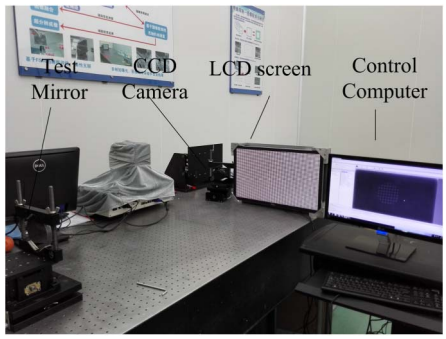

Fig. 3. Preliminary experimental device.

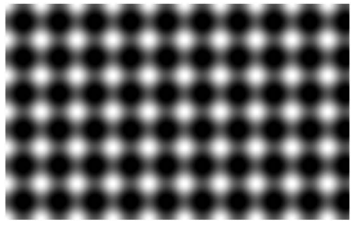

Fig. 4. Dual-frequency crossed fringe with reference points on LCD screen.

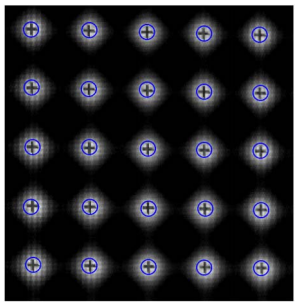

Fig. 5. Some reference points and re-projection points on the CCD image: +, reference points on the CCD image; O, re-projection points after bundle adjustment.

Table 1. Differences of Test Mirror Pixels (mm)

	X	Y	Z
RMS	3.675	2.356	0.532
PV	9.860	7.423	0.965

differences between the two groups of mirror pixels corresponding to the two groups of reflection ray directions shown in Table 1.

We fix the camera and place it in the CoC of the small test mirror. The regular fringe displayed on the LCD2 screen is reflected by the test sphere mirror, and the deformed fringe is captured by the fixed camera. With the reflection ray direction calibrated by the common method or the new method provided in this paper), the coordinates of the mirror corresponding to the camera pixels can be calculated. The coordinates of LCD2 can be computed by correspondence matching, and the recovered absolute phases of both the horizontal and vertical deformed fringes are shown in Fig. 6. With the coordinates of

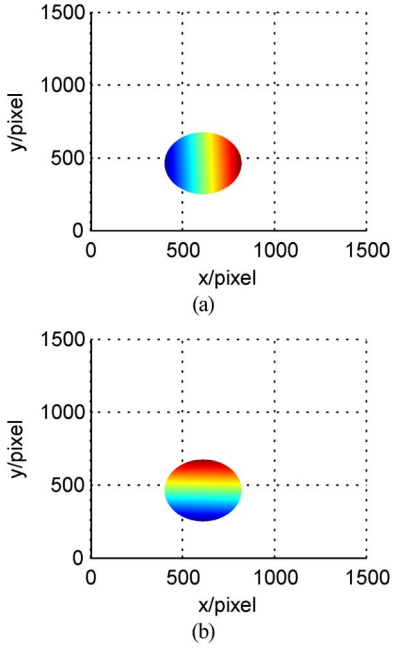

Fig. 6. Absolute phase distribution of (a) horizontal and (b) vertical deform fringes.

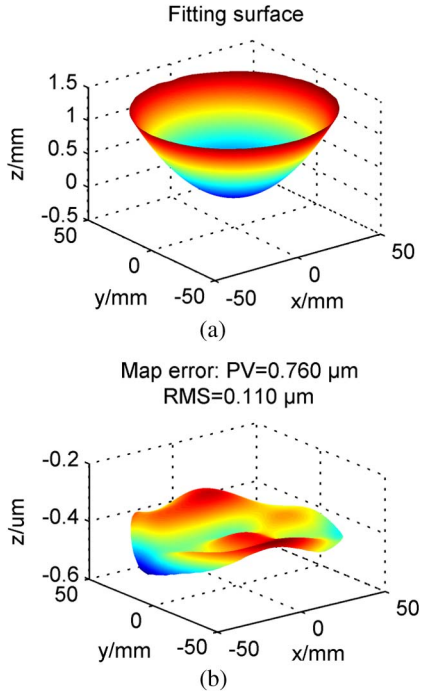

Fig. 7. (a) Specular shape by fringe-reflection measurement. (b) Mapped errors of fringe-reflection measurement.

the camera, LCD2, and the mirror, the slope can be computed by Eq. (1), and the three-dimensional shape can be reconstructed by model iteration. Figure 7(a) shows the three-dimensional reconstructed shape of a sphere mirror with common reflection ray direction calibration using one location of LCD1, and Fig. 7(b) shows the mapped error between the

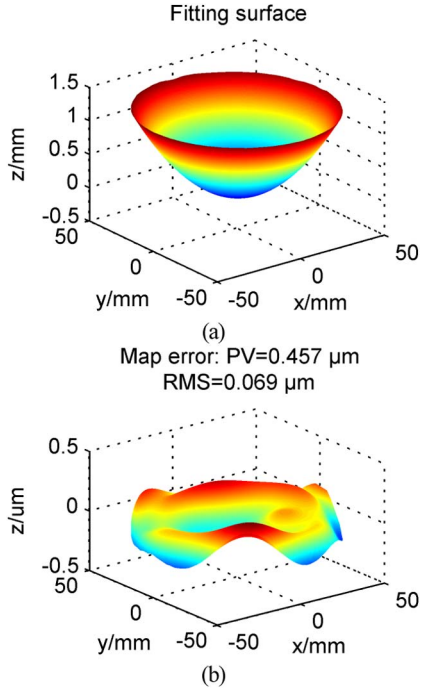

Fig. 8. (a) Specular shape after calibration. (b) Mapped errors of fringe-reflection measurement.

measurement results and the ideal shape, where the peak value (PV) equals 0.760 μm, and root mean square (RMS) equals 0.110 μm. Figure 8(a) shows the three-dimensional reconstructed shape of a sphere mirror with reflection ray direction calibration provided by this paper, and Fig. 8(b) shows the mapped error between the measurement results and the ideal shape, where the PV equals 0.457 μm, and the rms equals 0.068 μm. Compared with the two shape errors shown in Figs. 7(b) and 8(b), we can find that the error of shape is indeed reduced by using the method provided by this paper. In fact, the reflection ray directions are calibrated to find the initial mirror pixel coordinates, and the more precise the initial value is, the more accurate the final surface shape will be.

5. CONCLUSION

In conclusion, the trouble of geometrical calibration in fringe-reflection three-dimensional shape measurement is alleviated with the help of moving LCD1 near the test mirror and in front of the camera. Moving LCD1 along the optical axis of the test mirror once is sufficient to accomplish the calibration of reflection ray directions into the camera. It is demonstrated that the proposed method can be utilized simply and flexibly in a fringe-reflection measurement system. It is robust for the calibration of the test mirror.

Funding. National Natural Science Foundation of China (NSFC) (61036015).

Acknowledgment. Grateful thanks are also due to researchers Feng Zhang and Xiaoping Tao *et al.* in the Key Laboratory of Optical System Advanced Manufacturing Technology for their academic support and supervision.

REFERENCES

1. G. Häusler, C. Richter, K.-H. Leitz, and M. C. Knauer, "Microdeflectometry-a novel tool to acquire three-dimensional microtopography with nanometer height resolution," Opt. Lett. **33**, 396–398 (2008).
2. P. Su, R. E. Parks, L. Wang, R. P. Angel, and J. H. Burge, "Software configurable optical test system: a computerized reverse Hartmann test," Appl. Opt. **49**, 4404–4412 (2010).
3. P. Su, M. A. H. Khreishi, T. Su, R. Huang, M. Z. Dominguez, A. Maldonado, G. Butel, Y. Wang, R. E. Parks, and J. H. Burge, "Aspheric and freeform surfaces metrology with software configurable optical test system: a computerized reverse Hartmann test," Opt. Eng. **53**, 031305 (2014).
4. P. Su, Y. Wang, J. H. Burge, K. Kaznatcheev, and M. Idir, "Non-null full field X-ray mirror metrology using SCOTS: a reflection deflectometry approach," Opt. Express **20**, 12393–12406 (2012).
5. R. Huang, P. Su, T. Horne, G. Brusa, and J. H. Burge, "Optical metrology of a large deformable aspherical mirror using software configurable optical test system," Opt. Eng. **53**, 085106 (2014).
6. Z. Zhang, "A flexible new technique for camera calibration," IEEE Trans. Pattern Anal. Mach. Intell. **22**, 1330–1334 (2000).
7. R. Y. Tsai, "A versatile camera calibration technique for high-accuracy 3D machine vision metrology using off-the-shelf tv cameras and lenses," IEEE J. Robot. Autom. **3**, 323–344 (1987).
8. W. H. Southwell, "Wave-front estimation from wave-front slope measurements," J. Opt. Soc. Am. A **70**, 998–1006 (1980).
9. T. Bothe, W. Li, M. Schulte, C. von Kopylow, R. B. Bergmann, and W. P. O. Jüptner, "Vision ray calibration for the quantitative geometric description of general imaging and projection optics in metrology," Appl. Opt. **49**, 5851–5860 (2010).
10. R. E. Parks and W. P. Kuhn, "Optical alignment using the Point Source Microscope," Proc. SPIE **5877**, 58770B (2005).
11. Y.-L. Xiao, X. Su, W. Chen, and Y. Liu, "Three-dimensional shape measurement of aspheric mirrors with fringe reflection photogrammetry," Appl. Opt. **51**, 457–464 (2012).
12. Y. Liu, E. Olesch, Z. Yang, and G. Häusler, "Fast and accurate deflectometry with crossed fringes," Adv. Opt. Technol. **3**, 441–445 (2014).